Energy Conversion and Management 93 (2015) 435–447

Contents lists available at ScienceDirect

Energy Conversion and Management

journal homepage: www.elsevier.com/locate/enconman

Thermodynamic modeling of a hybrid solar gas-turbine power plant

D. Olivenza-León [a], A. Medina [a,*], A. Calvo Hernández [b]

[a] Departamento de Física Aplicada, Universidad de Salamanca, 37008 Salamanca, Spain
[b] Departamento de Física Aplicada and IUFFYM, Universidad de Salamanca, 37008 Salamanca, Spain

ARTICLE INFO

Article history:
Received 5 August 2014
Accepted 10 January 2015
Available online 30 January 2015

Keywords:
Thermosolar gas-turbines
Hybrid plants
Thermodynamic simulation
Global plant performance

ABSTRACT

A thermodynamic model for a hybrid solar gas-turbine power plant is presented. All the subsystems of the plant are modeled, taking into account the most important losses sources: those coming from heat losses in the solar subsystem, those in the combustion chamber, those associated to the Brayton cycle, and those heat losses in the heat exchangers connecting subsystems. Analytical expressions for the overall plant efficiency and its power output are obtained in a general form, for whichever solar share: from the pure combustion mode when solar irradiance is null or small, to the eventual case in which only solar heat input would be enough to ensure that the working fluid reaches the turbine inlet temperature. The gas-turbine model is validated by direct comparison of the model predictions with the output parameters of a commercial turbine. Results are very promising. The real parameters of an existing experimental thermosolar plant are considered and its performance records in stationary irradiance conditions are obtained. A sensitivity analysis of the influence of several turbine losses is performed: recuperator, turbine, compressor, and pressure losses. Finally, the influence of the pressure and temperature ratios on the overall plant efficiency and the fuel conversion rate is discussed. This kind of thermodynamic analysis is necessary in order to design efficient as well as commercially interesting new generations of plants of this type.

1. Introduction

Due to the rapid decrease of fossil fuel reserves and the international commitment for the reduction of pollutant emissions, alternative energy sources are being intensively sought. Solar energy is one of the candidate energy sources to at least partially substitute fossil fueled generation plants. But up to now generation costs for producing electric energy from pure thermosolar input are high compared to conventional production [1]. Moreover, there is an inherent problem related to guarantee a constant and predictable power delivery to the grid. One possible alternative are solar-fossil hybrid thermosolar power plants. Among them, those based on a Brayton gas-turbine scheme have additional advantages as reliability, quick start-up and shut-down processes, fully dispatchable power, and probably the most important, very low water consumption [2]. This is specially relevant in high solar irradiance areas usually linked to arid conditions.

All those reasons have led during the last years to important efforts to develop prototype and experimental plants to investigate the viability of the hybrid solar gas-turbine plant concept. Solar gas-turbine plants make use of concentrated solar power to heat pressurized air performing a Brayton cycle before entering the combustion chamber. The combustion chamber adds the required energy to cover the gap between the air temperature after receiving the solar input energy and the turbine inlet temperature. Modern recuperated gas-turbines are thus combined with an heliostat field through a solar receiver usually located in a central tower. From now on some key projects developed during the last years in this area are briefly summarized.

The SOLGATE (*Solar Hybrid Gas Turbine Electric Power System*) project [3–5] made use of the CESA1 solar tower and field installed at Plataforma Solar de Almería (Spain). Its objective was the development of a solar-hybrid power system with direct solar heating of pressurized air, as working fluid of a gas-turbine. A standard gas-turbine was modified for external air heating, pressurized receiver technology was investigated with the aim to get air outlet at temperatures up to 1000 °C, and software tools for simulating the system were developed. Experimental results in 2003 were considered as satisfactory. The project SOLHYCO (*Solar Hybrid Power and Cogeneration Plants*) [6] (2006-10) focused on the development of a 100 KWe prototype solar-hybrid microturbine system for cogeneration. It was based on a standard commercial microturbine and special emphasis was laid on the development of an up-to-date receiver based on a new high-performance tube

* Corresponding author. Tel.: +34 923 29 44 36; fax: +34 923 29 45 84.
E-mail addresses: olivenza.d@gmail.com (D. Olivenza-León), amd385@usal.es (A. Medina), anca@usal.es (A. Calvo Hernández).

http://dx.doi.org/10.1016/j.enconman.2015.01.027
0196-8904/

Nomenclature

A_a	aperture area of the collector
A_r	absorber area of the collector
a_c	isentropic compressor pressure ratio
a_t	isentropic turbine pressure ratio
C	solar collector concentration ratio
c_w	specific heat of the working fluid
DP	design point
f	solar share
G	solar irradiance
h_1	radiation heat loss coefficient for the solar collector
h_2	effective convection and conduction loss coefficient for the solar collector
$\dot{m}$	mass flow rate of the working substance
$\dot{m}_f$	fuel mass flow rate
ME	maximum efficiency
MP	maximum power output
P	power output
$\lvert\dot{Q}_{\mathrm{H}}\rvert$	total heat-transfer rate absorbed from the working fluid
$\lvert\dot{Q}_{\mathrm{HC}}\rvert$	heat input from the combustion chamber
$\lvert\dot{Q}_{\mathrm{LC}}\rvert$	heat losses in the combustion chamber
$\lvert\dot{Q}'_{\mathrm{HC}}\rvert$	heat rate transferred from the combustion chamber to the associated heat exchanger
$\lvert\dot{Q}'_{\mathrm{eHC}}\rvert$	heat losses in the combustion chamber heat exchanger
$\lvert\dot{Q}_{\mathrm{HS}}\rvert$	heat rate input from the solar collector
$\lvert\dot{Q}_{\mathrm{LS}}\rvert$	heat losses in the solar collector
$\lvert\dot{Q}'_{\mathrm{HS}}\rvert$	heat rate transferred from the solar collector to the associated heat exchanger
$\lvert\dot{Q}'_{\mathrm{eHS}}\rvert$	heat losses in the solar collector heat exchanger
$\lvert\dot{Q}_L\rvert$	heat-transfer rate between the working fluid and the ambient
Q_{LHV}	lower heating value of the fuel
r_e	fuel conversion rate
r_p	overall pressure ratio
T_{HC}	working temperature of the combustion chamber
T_{HS}	working temperature of the solar collector
T_L	ambient temperature (K)
t_L	ambient temperature (°F)
T_x	working fluid temperature after the heat input from the regenerator
T'_x	working fluid temperature after heat input from the solar collector
T_y	working fluid exhaust temperature
T_3	turbine inlet temperature
U_L	convective losses of the solar collector
α	effective emissivity
η	overall thermal efficiency
η_C	combustion chamber efficiency
η_{H}	thermal efficiency of the Brayton heat engine
$\varepsilon_{\mathrm{HC}}$	combustion chamber heat exchanger efficiency
$\varepsilon_{\mathrm{HS}}$	solar collector heat exchanger efficiency
η_S	solar collector efficiency
η_0	effective transmittance-absorptance product
ε_c	isentropic efficiency of the compressor
ε_L	cold side heat exchanger efficiency
ε_r	regenerator effectiveness
ε_t	isentropic efficiency of the turbines
γ	adiabatic coefficient of the working fluid
ρ_{H}	irreversibilities due to pressure drops in the heat input
ρ_L	irreversibilities due to pressure drops in the heat release
σ	Stefan–Boltzmann constant
τ_{HS}	temperature ratio associated to the solar collector
τ_{HC}	temperature ratio associated to the combustion chamber

technology. Different variations for cogeneration systems and combined cycle systems were analyzed together with the cost of the generated electricity. One of the main conclusions was that the economical feasibility of plants of this type requires an effort to get high-energy conversion efficiencies. More recently an international consortium, led by Abengoa Solar, take part in a project called SOLUGAS [7] in order to develop the first solar hybrid driven gas-turbine system on a pre-commercial scale. The project started in 2008 and has a duration of 54 months. The heliostat field used is the Solúcar platform (Sanlúcar La Mayor, Sevilla, Spain). SOLUGAS receiver is expected to heat compressed air to operation temperatures of 800 °C, and then the air is fed into the combustion chamber of a 4.6 MWe industrial gas-turbine.

Although all these technological projects show that during the last years a considerable effort from private organizations as well as public institutions has been made in order to develop these technologies, the basic research on these systems is still an open field. This is especially important since most prototype plants show the necessity of improving overall energy conversion efficiency in order to get a commercially suitable technology. Within this context, thermodynamic analyses of these plants are interesting in order to optimize the main parameters required to design future plants. They provide an integrated perspective of the plant subsystems and the contribution of each of them to the whole plant efficiency. This facilitates the detection of the main design and operation flaws, and provides a guide to obtain combinations of parameters reducing inefficiencies.

There exist in the specialized literature several research works on solar systems running in several thermodynamic cycles. Probably the most analyzed up to date, because of its practical interest is the Rankine solar cycle [8–10], but also other theoretical cycles were analyzed in order to predict the limits that thermodynamics imposes for the efficiency of solar driven systems. These include solar Carnot [11,12], Ericsson [13–15], Braysson [16–18], and Stirling [13,19,20] systems. Surprisingly, there are not many analyses of solar driven Brayton plants in spite of their potential commercial interest as commented above. Leroux et al. [21–23] have developed several works on these plants, specially on aspects related to the development and analysis of solar receivers. They have recently published a review on the subject [24]. Spelling et al. [25,26] have focused on the viability of this technology by working on thermoeconomic aspects. Other works rely on the use of commercial simulation programs as TRNSYS [27], from which it is difficult to extract general conclusions or to deep in the thermodynamics of these systems.

Usually thermodynamic models are far from reality because either do not incorporate all the main losses in real plants [16,28] or describe a purely solar (non-hybrid) plant operation [29–31]. Even more, to our knowledge there are no fully thermodynamic analytical analyses of hybrid plants that could work either with solar energy input or with the heat released by a combustion chamber. Thermodynamic studies allow a very helpful pre-design analysis in order to survey the effect of the main plant parameters in the plant output records and the importance of the several loss sources. Then, they can give a guide to find the optimum intervals for the parameters that would lead to optimize plant operation (in respect to its global efficiency, power output, or any other objective function). So, the main aim of this paper is to develop a full thermodynamic model for a solar-hybrid Brayton type plant incorporating the main irreversibility associated losses that a real plant

has. This analysis could be very useful in the future design of this type of hybrid solar plants, specially in the design optimization process required to increase its efficiency to make them interesting for commercial exploitation.

The paper is structured as follows. In Section 2 we set the main hypothesis of the model, obtain general equations for the overall efficiency of the plant, and detail the involved submodels: solar collector, combustion chamber, and Brayton heat engine. In Section 3 the model is validated by comparing its predictions with experimental measures for a commercial turbine. Section 4 is devoted to analyze the sensitivity of the efficiency and power output of the system to the basic parameters of the heat engine. In Section 5 the predictions of the model in which respect to the evolution of efficiencies with the solar collector and combustion temperature ratios are shown. Finally, the main conclusions of the analysis and the perspectives for future work are summarized.

2. Thermodynamic model and plant efficiency

An schematic representation of the considered hybrid plant is depicted in Fig. 1 and a diagram of the main energy fluxes is plotted in Fig. 2. The working fluid develops a closed Brayton like cycle. It is first compressed through a non-ideal compressor and then heated in three steps from two external sources. It receives a first energy input in a regenerator that makes use of the high temperature at the turbine exit, then a second heat input coming from a concentrating solar receiver, and eventually, a third heat input in order to ensure that the appropriate turbine inlet temperature is reached. After the regenerator exit, as the cycle is considered as closed, a heat exchanger releases a heat flux to the ambient, so the temperature at the compressor inlet is recovered.

In the scheme of Fig. 2 the heat engine system is shown with a green dotted line. It receives two external heat inputs, $\dot{Q}_{HS}$, and $\dot{Q}_{HC}$, coming respectively from the solar collector and the combustion chamber. The heat engine produces a power output, P, and releases a heat flux, $\dot{Q}_L$, to its surroundings. The whole system is enclosed in a black dashed line in Fig. 2. It includes the solar collector, combustion chamber, all the required heat exchangers and the heat engine itself. It receives two energy inputs: (a) A solar power input denoted by GA_a, where G is the mean solar irradiance and A_a, is the aperture area of the solar collector. The losses in the solar collector are denoted by $\dot{Q}_{LS}$ and will be detailed later. The useful heat flux, $\dot{Q}'_{HS}$, obtained from the collector is transferred to the working fluid through a solar receiver considered as non-ideal heat exchanger with efficiency ε_{HS}, so the effective solar heat flux received by the working fluid in the heat engine is $\dot{Q}_{HS}$. The losses in the solar heat exchanger are denoted by $\dot{Q}'_{eHS}$. (b) In a similar way, the combustion chamber transforms a global energy input $\dot{m}_f Q_{LHV}$, where $\dot{m}_f$ is the instantaneous fuel mass flow and Q_{LHV} its corresponding lower heating value, into a useful work $\dot{Q}_{HC}$ received by the working fluid. In order to have an alike scheme that in the solar subsystem, we consider separately losses in the combustion chamber itself, $\dot{Q}_{LC}$ (associated to incomplete combustion and losses through its walls) and losses in the heat exchanger that transfers the heat to the working fluid. It has an isentropic efficiency ε_{HC} and the corresponding losses are $\dot{Q}'_{eHC}$.

The thermal efficiency of the whole system, η, is defined as the ratio between the net mechanical power output, P, and the total heat input rate, that has two energy sources: solar and combustion of a conventional (fossil or bio-) fuel,

$$\eta = \frac{P}{GA_a + \dot{m}_f Q_{LHV}} \tag{1}$$

Our purpose now is to express this global efficiency in terms of the efficiency of the solar collector, η_S, that of the combustion chamber, η_C, the efficiency of the Brayton heat engine, η_H, and the efficiencies of all the required heat exchangers to transfer the heat flows in or out of the working fluid.

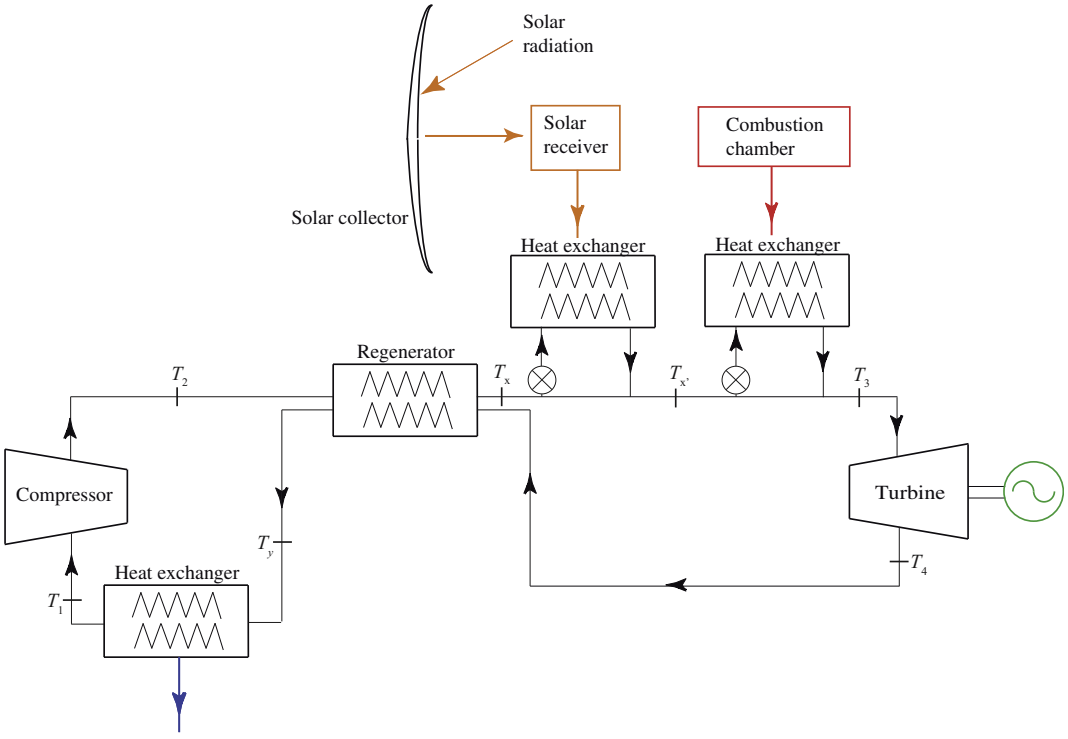

Fig. 1. Scheme of the hybrid solar gas-turbine plant considered.

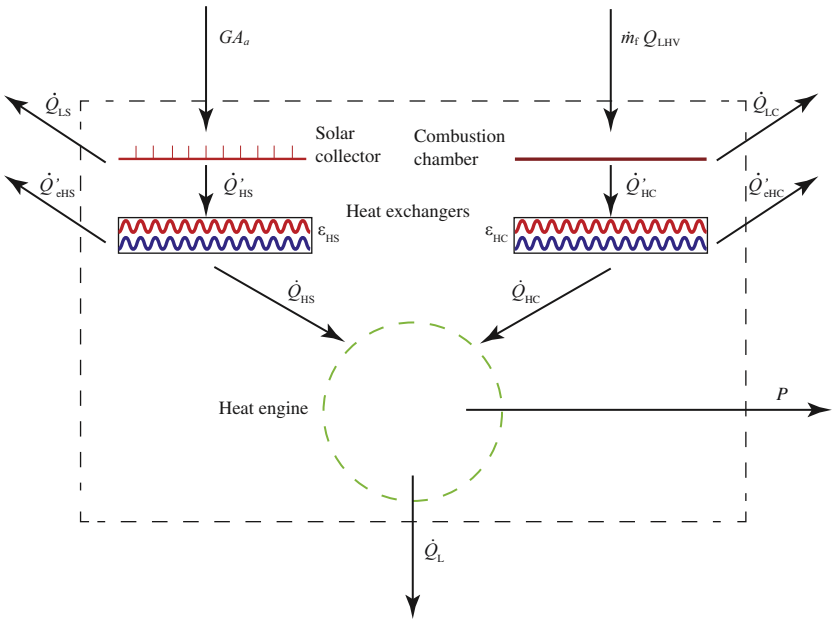

Fig. 2. Main energy fluxes in the plant. The heat engine (HE) is encompassed with a dotted green line and the whole system with a black dotted line. The latter includes the heat engine itself, the solar subsystem, the combustion chamber, and all the required heat exchangers. The heat engine produces a power output P and releases a heat flux $\dot{Q}_L$ to its surroundings. (For interpretation of the references to colour in this figure legend, the reader is referred to the web version of this article.)

The efficiency of the solar collector, η_S, is defined as the ratio between the useful heat rate that the collector provides, $|\dot{Q}'_{HS}|$, and the solar energy rate it receives, GA_a:

$$\eta_S = \frac{|\dot{Q}'_{HS}|}{GA_a} \tag{2}$$

The working fluid that performs the thermal cycle receives the solar heat input through a solar receiver, that transfers a heat rate $|\dot{Q}_{HS}|$ to the working fluid. The solar receiver can be characterized by an isentropic efficiency, $\varepsilon_{HS} = |\dot{Q}_{HS}|/|\dot{Q}'_{HS}|$. So, the efficiency of the solar collector can be expressed in terms of the heat rate received by the fluid, $|\dot{Q}_{HS}|$, and the efficiency of the receiver, ε_{HS}, as:

$$\eta_S = \frac{|\dot{Q}_{HS}|/\varepsilon_{HS}}{GA_a} \tag{3}$$

The working temperature of the solar collector is denoted as T_{HS}, the temperature of the gas after the regenerator is T_x, and the temperature after the solar input is T'_x (for notation, see Fig. 1).

In a similar way, the combustion chamber generates a heat rate, $|\dot{Q}'_{HC}|$, that is transferred to the working fluid by means of a heat exchanger with isentropic efficiency $\varepsilon_{HC} = |\dot{Q}_{HC}|/|\dot{Q}'_{HC}|$, so the working fluid receives a heat rate $|\dot{Q}_{HC}|$ coming from the combustion of the fuel. Note that a closed Brayton cycle is being modeled, so the fuel is not injected in the air itself, but the gas receives the energy input coming from combustion through a heat exchanger. The efficiency of the combustion chamber is thus given by:

$$\eta_C = \frac{|\dot{Q}'_{HC}|}{\dot{m}_f Q_{LHV}} = \frac{|\dot{Q}_{HC}|/\varepsilon_{HC}}{\dot{m}_f Q_{LHV}} \tag{4}$$

The temperature at the entrance of the heat exchanger associated to the combustion chamber is that at the outlet of the solar energy input, T'_x, and the outlet temperature is the turbine inlet temperature, T_3.

The thermal efficiency of the heat engine is defined as usual, as the ratio between the net power output, P, and the total heat input received by the working fluid, $|\dot{Q}_H| = |\dot{Q}_{HS}| + |\dot{Q}_{HC}|$:

$$\eta_H = \frac{P}{|\dot{Q}_{HS}| + |\dot{Q}_{HC}|} \tag{5}$$

In Section 2.2 it will be detailed the main hypotheses of the gas-turbine model in which respect to the irreversibility sources considered and explicit calculations of the heat engine efficiency in terms of the main cycle variables and parameters quantifying losses will be shown.

For the calculation of the overall efficiency of the whole system we substitute Eqs. (3) and (4) in Eq. (1), so

$$\eta = \frac{P}{\frac{|\dot{Q}_{HS}|}{\varepsilon_{HS}\eta_S} + \frac{|\dot{Q}_{HC}|}{\varepsilon_{HC}\eta_C}} = \eta_S\eta_C\eta_H\left(\frac{|\dot{Q}_{HS}| + |\dot{Q}_{HC}|}{\eta_C\frac{|\dot{Q}_{HS}|}{\varepsilon_{HS}} + \eta_S\frac{|\dot{Q}_{HC}|}{\varepsilon_{HC}}}\right) \tag{6}$$

Defining a solar share ratio as the ratio of the solar heat rate that the working fluid absorbs with respect to the total heat input, $f = |\dot{Q}_{HS}|\Big/\left(|\dot{Q}_{HS}| + |\dot{Q}_{HC}|\right)$, the efficiency can be expressed as:

$$\eta = \eta_S\eta_C\eta_H\left[\frac{1}{\frac{\eta_C f}{\varepsilon_{HS}} + \frac{\eta_S(1-f)}{\varepsilon_{HC}}}\right] = \eta_S\eta_C\eta_H\left[\frac{\varepsilon_{HS}\varepsilon_{HC}}{\eta_C\varepsilon_{HC}f + \eta_S\varepsilon_{HS}(1-f)}\right] \tag{7}$$

This equation gives us the global efficiency in terms of the thermal efficiency of the solar collector, η_S, the combustion chamber, η_C, the heat engine, η_H, the solar share, f, and the isentropic efficiencies of the heat exchangers the working fluid receives the heat input through, ε_{HS} and ε_{HC}. This expression is valid for the general case when both heat sources are simultaneously releasing energy to the fluid. In the particular case in which eventually all the energy input comes from the solar collector, $f = 1$, and $\eta = \eta_S\eta_H\varepsilon_{HS}$, and when solar irradiance is null, and the turbine works only with the heat released in the combustion reactions, $f = 0$, and $\eta = \eta_C\eta_H\varepsilon_{HC}$.

It is also interesting to define a performance relative to the energy input with an economical cost, *i.e.*, to the fuel burned. It constitutes a *fuel conversion rate*, and can be defined as suggested by Heywood [32]:

$$r_e = \frac{P}{\dot{m}_f Q_{LHV}} \tag{8}$$

It can be related with the efficiency of the global system, η, and the efficiencies of the solar subsystem, η_S, and the heat engine, η_H through Eqs. (1)–(3), Eq. (5) and the definition of solar share, f. It is easy to show that:

$$r_e = \frac{\eta\,\eta_S\eta_H\varepsilon_{HS}}{\eta_S\eta_H\varepsilon_{HS} - \eta f} \tag{9}$$

In the case that all the energy input comes from combustion, $f = 0$ and $r_e = \eta$. In the opposite situation, if eventually all the energy was solar, $f = 1$ and $\eta = \eta_S\eta_H\varepsilon_{HS}$, so $r_e \to \infty$. Thus, note that this rate is defined in the interval $[0,\infty]$, not in the interval $[0,1]$ or $[0,\eta_{Carnot}]$, where η_{Carnot} represents the corresponding Carnot's efficiency, as it happens for thermodynamic efficiencies. Strictly it is not a thermodynamic efficiency, it is a measure of the system performance from the viewpoint of fuel costs. In a solar hybrid system as the one considered here, r_e, can reach values over 1 because a fraction of the energy input has not associated costs.

2.1. Modeling subsystems: solar plant and combustion chamber

In order to model the heat released from the solar collector, $|\dot{Q}'_{HS}|$ and its efficiency, η_S, it is assumed that at low and intermediate collector temperatures the losses at the collector essentially comes from conduction and convection, while at sufficiently high temperatures main losses comes from radiation. The energy collected at the aperture is GA_a, and the useful energy provided by the solar plant is the difference between the energy transmitted to the receptor, $\eta_0 GA_a$, where η_0 is the effective transmittance-absorptance product (optical efficiency) and the losses, $|\dot{Q}_{LS}|$, that in general contain a linear term in temperature differences accounting for conduction and convection losses and a term on the fourth power of the collector temperature, T_{HS}, associated to radiation losses. Thus, the useful heat released from the collector and its efficiency can be respectively expressed, as [18,33–35]:

$$|\dot{Q}'_{HS}| = \eta_0 GA_a - \alpha\sigma A_r T_L^4(\tau_{HS}^4 - 1) - U_L A_r T_L(\tau_{HS} - 1) \tag{10}$$

$$\eta_S = \frac{|\dot{Q}'_{HS}|}{GA_a} = \frac{|\dot{Q}_{HS}|/\varepsilon_{HS}}{GA_a} = \eta_0\left[1 - h_1 T_L^4(\tau_{HS}^4 - 1) - h_2 T_L(\tau_{HS} - 1)\right] \tag{11}$$

In these equations $\tau_{HS} = T_{HS}/T_L$ denotes the ratio between the working temperature of the solar collector and the ambient, A_a and A_r are, respectively, the aperture and absorber areas, $h_1 = \alpha\sigma/(\eta_0 GC)$, $h_2 = U_L/(\eta_0 GC)$, where U_L is the convective heat loss coefficient, α is the effective emissivity of the collector, $C = A_a/A_r$ is the concentration ratio, and σ the Stefan–Boltzmann constant. By considering $h_2 = 0$ the model with purely radiative losses is recovered [36].

The efficiency of the combustion chamber is given by Eq. (4). For most applications, once elected the fuel to be burned, it could be considered as a constant parameter. The heat received by the working fluid from the combustion chamber, $\dot{Q}_{HC}$, can be written as:

$$|\dot{Q}_{HC}| = \varepsilon_{HC}|\dot{Q}'_{HC}| = \varepsilon_{HC}\,\eta_C\,\dot{m}_f\,Q_{LHV} \tag{12}$$

In terms of temperatures:

$$|\dot{Q}_{HC}| = \dot{m}\,c_w(T_3 - T_{x'}) = \dot{m}\,c_w\,\varepsilon_{HC}(T_{HC} - T_{x'}) \tag{13}$$

where $\dot{m}$ is the working fluid mass flow and c_w is its specific heat. The effective temperature in the combustion chamber is denoted as T_{HC}, and the associated temperature ratio as $\tau_{HC} = T_{HC}/T_L$. In the numerical applications that will be considered later in this work stationary solar conditions will be taken for the irradiance, so the temperature T'_x will be constant, but in the general eventual case that G is oscillating (and so T'_x) with the hours in a day and with the weather and seasonal conditions, the fuel mass flow to be burned in the combustion chamber is in general given by:

$$\dot{m}_f = \frac{\dot{m}\,c_w(T_3 - T_{x'})}{\eta_C\,Q_{LHV}\,\varepsilon_{HC}} \tag{14}$$

The rate of fuel mass burned can be also obtained from the fuel conversion rate defined in Eq. (9):

$$\dot{m}_f = \frac{P}{r_e\,Q_{LHV}} \tag{15}$$

2.2. Modeling subsystems: Brayton gas-turbine

In this section the efficiency of the heat engine, η_H, is obtained by considering that it develops an irreversible closed recuperative Brayton cycle. The $T-S$ diagram of the cycle is depicted in Fig. 3. We suppose that the working fluid is a mass flow $\dot{m}$ of an ideal gas with constant specific heat, c_w. Although this is a restrictive hypothesis, as elsewhere commented in the literature [18] due to the large temperature changes experienced by the gas, it is assumed in order to obtain analytical expressions for the heat inputs and the efficiency. For numerical applications, an approximate value for c_w or the adiabatic coefficient, γ, will be calculated by averaging the corresponding temperature dependent polynomials in the adequate temperature interval.

(1) As described above, the cycle for the gas begins with a compression (1→ 2) by means of a non-ideal compressor, which isentropic efficiency is given by:

$$\varepsilon_c = \frac{T_{2s} - T_1}{T_2 - T_1} \tag{16}$$

In this equation T_{2s} represents the temperature of the working fluid after the compression process if it was adiabatic and T_2 is the actual temperature at the compressor outlet.

(2) Between states 2 and 3 (process 2 → 3), in general the gas sequentially receives three energy inputs. First, the non-ideal regenerator is capable to increase the gas temperature from T_2 to T_x. Its effectiveness, ε_r, is defined as the ratio between the actual temperature $(T_x - T_2)$ increase and the ideal maximum one $(T_4 - T_2)$:

$$\varepsilon_r = \frac{T_x - T_2}{T_4 - T_2} = \frac{T_y - T_4}{T_2 - T_4} \tag{17}$$

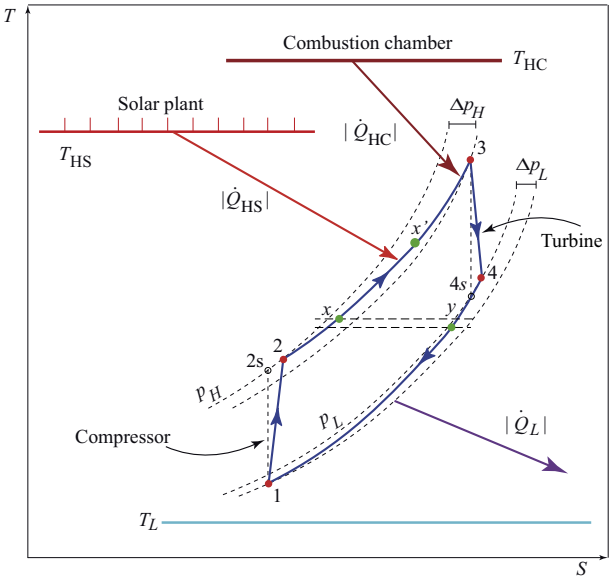

Fig. 3. $T-S$ diagram of the irreversible Brayton cycle experienced by the working fluid. Several irreversibility sources are considered (see text).

In the case of a non-recuperative cycle, $\varepsilon_r = 0$, and in the limit case of an ideal recuperator with no losses, its effectiveness equals the unity, $\varepsilon_r = 1$. The consideration of ε_r as a variable for the global efficiency or other output parameters of the plant would allows us to analyze to which extent an investment in a good regenerator increases the plant output parameters.

Second, the gas receives a heat flow, $|\dot{Q}_{HS}|$, from the solar subsystem (step $x \to x'$) and thus its temperature increases from T_x to T'_x. The isentropic efficiency, ε_{HS}, of the heat exchanger connecting the working fluid with the solar subsystem in terms of temperatures is given by:

$$\varepsilon_{HS} = \frac{T_{x'} - T_x}{T_{HS} - T_x} \tag{18}$$

And third, in a similar way, the gas receives a completing heat input from the combustion chamber ($x' \to 3$) in order to ensure an approximately constant turbine inlet temperature, T_3, independently of the solar irradiance conditions. This is done through a heat exchanger with efficiency:

$$\varepsilon_{HC} = \frac{T_3 - T_{x'}}{T_{HC} - T_{x'}} \tag{19}$$

In which respect to the pressure during the heat addition processes, a global parameter, ρ_H, that quantifies the pressure decrease in the process $2 \to 3$ is considered. In real plants pressure decays are associated to the equipment in the three steps of the heat input process, so the curve $2 \to 3$ would not be as smooth as it is plotted in Fig. 4. But the consideration of a unique global pressure decay parameter allows to obtain analytical equations and to numerically check the effects of pressure decays in the output parameters of the plant. So, ρ_H is defined as:

$$\rho_H = \left(\frac{p_H - \Delta p_H}{p_H}\right)^{(\gamma-1)/\gamma} \tag{20}$$

where p_H is the highest pressure of the gas and $p_H - \Delta p_H$ its pressure at the turbine inlet.

(3) In the state 3 the working fluid has reached its maximum temperature and its is expanded by means of a non-ideal turbine during the power stroke ($3 \to 4$). In Fig. 3 the state 4s represents the final state in the ideal case the turbine acts as isentropic, and the state 4 is the actual final state after expansion. The isentropic efficiency of the turbine, ε_t is given by:

$$\varepsilon_t = \frac{T_{4s} - T_3}{T_4 - T_3} \tag{21}$$

(4) Finally, the gas recovers the conditions at the initial state 1 by releasing heat in the process $4 \to 1$ through two steps. First, by means of the regenerator (process $4 \to y$) and later by releasing heat to the ambient at temperature T_L through a non-ideal heat exchanger with efficiency, ε_L (process $y \to 1$):

$$\varepsilon_L = \frac{T_1 - T_y}{T_L - T_y} \tag{22}$$

The pressure loss during the whole heat release process is measured through a coefficient ρ_L given by:

$$\rho_L = \left(\frac{p_L - \Delta p_L}{p_L}\right)^{(\gamma-1)/\gamma} \tag{23}$$

where p_L is the gas pressure at the turbine outlet and $p_L - \Delta p_L$ its lowest pressure during the cycle. It is convenient to define a global pressure ratio, r_p as:

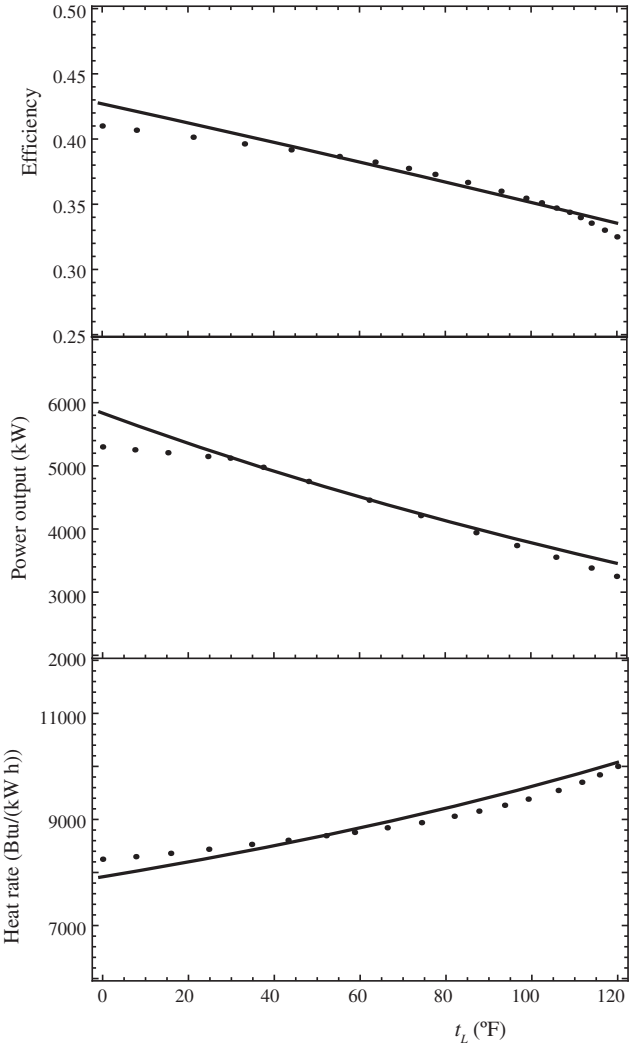

Fig. 4. Evolution with the external temperature, t_L, of the efficiency, power output, and heat rate for the turbine Mercury 50 as provided by the manufacturer [37] (dots) and calculated from our model (solid lines). Units are the same that those given by the producer.

$$r_p = \frac{p_H}{p_L - \Delta p_L} \tag{24}$$

Provided that the processes $1 \to 2s$ and $3 \to 4s$ are adiabatic (see Fig. 4), two parameters, a_c and a_t, related to the pressure ratios of the compressor and the turbine respectively are defined:

$$a_c = \frac{T_{2s}}{T_1} = \left(\frac{p_H}{p_L - \Delta p_L}\right)^{(\gamma-1)/\gamma} = r_p^{(\gamma-1)/\gamma} \tag{25}$$

$$a_t = \frac{T_3}{T_{4s}} = \left(\frac{p_H - \Delta p_H}{p_L}\right)^{(\gamma-1)/\gamma} \tag{26}$$

From Eqs. (20), (23), and (24) it is easy to find a relationship between them:

$$a_t = a_c \rho_H \rho_L \tag{27}$$

2.3. Heat flows and thermal efficiency for the Brayton gas-turbine

The purpose of this section is to express the heat flows received and released by the working fluid, $|\dot{Q}_{HS}|$, $|\dot{Q}_{HC}|$, and $|\dot{Q}_L|$ in terms of the parameters that quantify the irreversibility losses considered

in the model. From them it is straightforward to obtain the power output, P, and the thermal efficiency, η_H, of the heat engine.

First, we express the temperatures of all the states in the cycle in terms of the temperature of the solar collector, T_{HS}, that of the combustion chamber, T_{HC}, and the pressure ratios of the compressor, a_c and the turbine, a_t. By using the definitions in the section above, Eqs. (16)–(27), it is possible to obtain the following set of equations:

$$T_1 = \varepsilon_L T_L + T_y(1-\varepsilon_L) \tag{28}$$

$$T_2 = T_1 + \frac{1}{\varepsilon_c}(T_{2s} - T_1) = T_1 Z_c \tag{29}$$

$$T_3 = \varepsilon_{HC} T_{HC} + T_{x'}(1-\varepsilon_{HC}) \tag{30}$$

$$T_4 = T_3 - \varepsilon_t(T_3 - T_{4s}) = T_3 Z_t \tag{31}$$

$$T_x = \varepsilon_r T_4 + T_2(1-\varepsilon_r) \tag{32}$$

$$T_y = \varepsilon_r T_2 + T_4(1-\varepsilon_r) \tag{33}$$

$$T_{x'} = \varepsilon_{HS} T_{HS} + T_x(1-\varepsilon_{HS}) \tag{34}$$

The Eqs. (29) and (31) were simplified by introducing two definitions:

$$Z_c = 1 + \frac{1}{\varepsilon_c}(a_c - 1) \tag{35}$$

$$Z_t = 1 - \varepsilon_t\left(1 - \frac{1}{a_t}\right) \tag{36}$$

By simultaneously using Eqs. (28)–(34) it is feasible to express all the temperatures in terms of the temperatures of the heat sources, T_{HS} and T_{HC}, the ambient temperature, T_L, the pressure ratio, r_p and all the irreversibility parameters defined above. After cumbersome calculations, the following relationships are obtained:

$$T_2 = \frac{(1-\varepsilon_L)(1-\varepsilon_r)[\varepsilon_{HC}T_{HC} + \varepsilon_{HS}T_{HS}(1-\varepsilon_{HC})] + \varepsilon_L T_L\left[Z_t^{-1} - (1-\varepsilon_{HC})(1-\varepsilon_{HS})\varepsilon_r\right]}{\left[Z_c^{-1} - (1-\varepsilon_L)\varepsilon_r\right]\left[Z_t^{-1} - (1-\varepsilon_{HC})(1-\varepsilon_{HS})\varepsilon_r\right] - (1-\varepsilon_{HC})(1-\varepsilon_{HS})(1-\varepsilon_L)(1-\varepsilon_r)^2} \tag{37}$$

$$T_4 = \frac{[\varepsilon_{HC}T_{HC} + \varepsilon_{HS}T_{HS}(1-\varepsilon_{HC})]\left[Z_c^{-1} - (1-\varepsilon_L)\varepsilon_r\right] + \varepsilon_L T_L(1-\varepsilon_{HC})(1-\varepsilon_{HS})(1-\varepsilon_r)}{\left[Z_c^{-1} - (1-\varepsilon_L)\varepsilon_r\right]\left[Z_t^{-1} - (1-\varepsilon_{HC})(1-\varepsilon_{HS})\varepsilon_r\right] - (1-\varepsilon_{HC})(1-\varepsilon_{HS})(1-\varepsilon_L)(1-\varepsilon_r)^2} \tag{38}$$

$$\frac{T_3}{T_L} = \frac{T_4}{T_L} Z_t^{-1} = Z_t^{-1} \frac{[\tau_{HC}\varepsilon_{HC}(1-\varepsilon_{HC})\varepsilon_{HS}\tau_{HS}]\left[Z_c^{-1} - (1-\varepsilon_L)\varepsilon_r\right] + \varepsilon_L(1-\varepsilon_{HC})(1-\varepsilon_{HS})(1-\varepsilon_r)}{\left[Z_c^{-1} - (1-\varepsilon_L)\varepsilon_r\right]\left[Z_t^{-1} - (1-\varepsilon_{HC})(1-\varepsilon_{HS})\varepsilon_r\right] - (1-\varepsilon_{HC})(1-\varepsilon_{HS})(1-\varepsilon_L)(1-\varepsilon_r)^2} \tag{39}$$

$$\frac{T_1}{T_L} = \frac{\varepsilon_L + Z_t(1-\varepsilon_L)(1-\varepsilon_r)\frac{T_3}{T_L}}{1-\varepsilon_r(1-\varepsilon_L)Z_c} \tag{40}$$

$$\frac{T_x}{T_L} = \frac{T_4}{T_L}\varepsilon_r + \frac{T_2}{T_L}(1-\varepsilon_r) = \frac{T_3}{T_L} Z_t \varepsilon_r + \frac{T_1}{T_L} Z_c(1-\varepsilon_r) \tag{41}$$

It is easy to get the temperature of the working fluid at the recuperator exit by substituting Eqs. (37) and (38) in Eq. (33). The total heat input rate, $|\dot{Q}_H|$, and, the heat release, $|\dot{Q}_L|$, are expressed in terms of the temperatures in the following way:

$$|\dot{Q}_H| = |\dot{Q}_{HS}| + |\dot{Q}_{HC}| = \dot{m}c_w(T_3 - T_x) \tag{42}$$

$$|\dot{Q}_L| = \dot{m}c_w(T_y - T_1) \tag{43}$$

where,

$$|\dot{Q}_{HS}| = \dot{m}c_w(T_{x'} - T_x) = f|\dot{Q}_H| \tag{44}$$

$$|\dot{Q}_{HC}| = \dot{m}c_w(T_3 - T_{x'}) = (1-f)|\dot{Q}_H| \tag{45}$$

From the calculations above it is viable to obtain expressions for $|\dot{Q}_{HS}|, |\dot{Q}_{HC}|$, and $|\dot{Q}_L|$ in terms of the temperature ratios, τ_{HS}, τ_{HC}, the pressure ratio, r_p, and all the parameters accounting for irreversibilites. This is done by substituting Eqs. (39)–(41) in Eqs. (42)–(45) provided that the ratios $T_3/T_L, T_1/T_L$, and T_x/T_L can be expressed in terms of the mentioned temperature and pressure ratios, and the parameters associated to losses. Finally, the relevant heat rates are:

$$|\dot{Q}_{HS}| = \dot{m}c_w T_L \varepsilon_{HS}\left(\tau_{HS} - \frac{T_x}{T_L}\right) = \dot{m}c_w T_L \varepsilon_{HS}\left[\tau_{HS} - Z_t\varepsilon_r\frac{T_3}{T_L} - Z_c(1-\varepsilon_r)\frac{T_1}{T_L}\right] \tag{46}$$

$$|\dot{Q}_{HC}| = \dot{m}c_w T_L \varepsilon_{HC}\left\{\tau_{HC} - \tau_{HS}\varepsilon_{HS} - (1-\varepsilon_{HS})\left[\frac{T_3}{T_L}Z_t\varepsilon_r + \frac{T_1}{T_L}Z_c(1-\varepsilon_r)\right]\right\} \tag{47}$$

$$|\dot{Q}_L| = \dot{m}c_w T_L \varepsilon_L\left[\frac{T_3}{T_L}Z_t(1-\varepsilon_r) + \frac{T_1}{T_L}Z_c\varepsilon_r - 1\right] \tag{48}$$

Thus, the power output released by the heat engine, $P = |\dot{Q}_H| - |\dot{Q}_L|$, and its thermal efficiency, $\eta_H = P/|\dot{Q}_H|$, have analytical expressions susceptible to be evaluated for any set of the involved variables.

Gathering all the calculations, the efficiency of the heat engine, η_H [Eqs. (46)–(48)] and the efficiency of the solar subsystem, η_S [Eq. (11)] have been expressed analytically in terms of temperature and pressure ratios, and parameters accounting for the particular irreversibilities in each of them. For the efficiency of the combustion chamber an approximately constant given value, η_C will be considered. So, from the Eq. (7) that gives us the overall thermal efficiency, η, we are in conditions to obtain its numerical values after assuming a particular set of all the parameters mentioned above.

Some observations about the available temperature intervals for T_{HS} and T_{HC} are in order at this point:

- The solar share, f defined as the ratio between the solar heat rate received by the working fluid, $|\dot{Q}_{HS}|$ and the total heat input, $|\dot{Q}_H|$, in our work does not appear as an independent parameter, but it is a function of the temperatures of the heat sources, and all the other parameters.
- As a consequence of the assumptions made in this model for the sequence of heat absorption processes, the following inequalities for temperatures hold (see Fig. 3):

$$T_3 \geqslant T'_x \geqslant T_x \tag{49}$$

$$T_{HS} \geqslant T_x \tag{50}$$

$$T_{HC} \geqslant T'_x \tag{51}$$

Eq. (49) is trivially obtained from Eqs. (44) and (45). The equality $T_3 = T'_x$ is valid when solar radiation is capable to provide enough energy to the gas to reach the turbine inlet temperature. In terms of the solar share, $f = 1$. The equality $T'_x = T_x$ appears in the opposite case, all the energy comes from combustion, so the solar share is zero. The other equations, Eqs. (50) and (51), come from the fact that the efficiencies of the heat exchangers, ε_{HS} and ε_{HC} are greater than 0, Eqs. (18) and (19). The equalities holds in the case of ideal heat exchangers with no losses, $\varepsilon_{HS} = 1$ and/or $\varepsilon_{HC} = 1$.

3. Model validation

For the validation of the model a particular real plant was elected, the one developed in the SOLUGAS (*Solar Up-Scale Gas Turbine System*) project [7]. This project started in 2008 under the European Commission's 7th Framework Program. The spanish company Abengoa Solar led an international consortium with the objective to develop the first solar-driven gas-turbine plant on a

pre-commercial scale. It was constructed in one of the heliostat fields of Abengoa Solar in Sanlúcar la Mayor, Sevilla, Spain. The main objectives of this project, after some previous ones like SOLGATE and SOLHYCO, that showed the technical viability of this technology, was to demonstrate the performance and costs level of this kind of plants on a commercial scale and the persistence of its components, specially the solar receiver. With those objectives a 75 meter high concrete tower was designed and built to allocate the receiver and the gas-turbine. The heliostats field consists of 69 units designed by Abengoa, each of them of 121 m^2 reflective area and with an innovative tracking system. It is able to deliver more than 5 MWth.

The gas-turbine was placed in the central tower and was a commercial one, the *Mercury* 50 gas-turbine generator set manufactured by Solar Turbines [37]. It is considered as one of the lowest emitting and highest efficiency gas-turbine in its power size range. It is a recuperated gas-turbine with a power output of 4.6 MWe and 38.5% efficiency. In most applications is fed with natural gas.

To validate our model in which respect to the gas-turbine itself, some technical data given by the manufacturer and numerically calculated the main output parameters were collected. In Table 1 the experimental parameters are summarized together with those we had to assume to obtain numerical values, and the comparison between the experimental results and the numerical ones. In reference to our assumptions, the working fluid was considered air with averaged values of constant pressure specific heat, c_w, and adiabatic constant, γ. To calculate averages an standard polynomical form for $c_w(T)$ was considered [38] and averages were performed in the interval $[T_L, T_3]$. To account for the losses in the turbine, compressor and regenerator, realistic values of the corresponding isentropic efficiencies ($\varepsilon_t, \varepsilon_c$, and ε_r respectively) were taken. The global pressure losses in the heat absorption and heat release processes were taken identical and numerically around 11%, which leads to values of ρ_H and ρ_L through Eqs. (20) and (23) of 0.97. The manufacturer gives the output values at the generator terminals, so to compare with our results a 99% efficiency in the mechanical–electrical power conversion [39] was assumed. With all these assumptions, the comparison with the available real data: the temperature at the turbine inlet, T_3, the temperature after the regenerator, T_y, the efficiency, η_H, and the power output, P show a fairly good agreement with those of the real turbine as shown in the Table 1. In the worst case difference does not exceed 1.4%.

It is also plotted the evolution of the efficiency, power output, and heat rate (heat input required to obtain a certain power output) with the ambient temperature, T_L, and compared the result with those provided by the manufacturer for the turbine *Mercury* 50 [37]. These plots are shown in Fig. 4 in the same units and the same temperature interval (approximately between −18 °C and 49 °C) that in the turbine specifications. Again, the agreement between estimated and experimental results is notably satisfactory. Experimental curves show a behavior not so close to a linear one as predicted by the model, but numerical differences are small, being more apparent at small temperatures. At intermediate temperatures (between 40 and 80 °F, *i.e.*, between 4 and 26 °C), numerical differences are really scarce.

Unfortunately, we are not aware neither of the publication of a complete set of results for the project SOLUGAS when the plant is running in a fully hybrid mode, nor some details of the solar subsystem. So, some parameters (see Table 2) were assumed from those of similar facilities owned by Abengoa Solar in the same location (optical efficiency, concentration ratio, and design point irradiance) [7,46] and other were taken from standard values in the literature [18,28,40,41].

The working temperature of the solar collector was obtained by balancing the useful energy released by the solar collector, $\epsilon_{HS}|\dot{Q}'_{HS}|$, Eq. (10), and the heat input in the Brayton engine, $|\dot{Q}_{HS}|$, Eq. (46). This is depicted in Fig. 5. The first is a decreasing function of τ_{HS} in which losses increase due to radiation and convection-conduction terms. The second is a linearly increasing function of τ_{HS}. The crossing between them determines the effective working temperature of the solar collector. For an external temperature $T_L = 288$ K, it leads to $T_{HS} = 1088$ K. This is in accordance with the estimations for the SOLUGAS plant. To reach temperatures around this one was one of the objectives of the considered project

Table 1
Comparison of manufacturer's output results for the turbine *Mercury 50* (Solar Turbines, Caterpillar) [37] and the predictions of our model with the irreversibility set of parameters shown. The specifications give the efficiency and power output as measured as generator terminals. In our computations, it was assumed that the generator efficiency amounts 0.99%.

Mercury 50 manufacturer's specifications			
$\dot{m} = 17.9$ kg/s	$r_p = 9.9$	$T_L = 288$ K	
Measured output parameters			
$T_3 = 1423$ K	$T_y = 647$ K	$\eta = 0.385$	$P = 4.6$ MW
Assumed losses parameters			
$\varepsilon_{HC} = 0.98$	$\rho_H = \rho_L = 0.97$	$\varepsilon_t = 0.885$	$\varepsilon_r = 0.775$
$\varepsilon_L = 1$		$\varepsilon_c = 0.815$	
Calculated values			
$T_3 = 1418$ K	$T_y = 650$ K	$\eta_H = 0.387$	$P = 4.5$ MW

Relative deviations

T_3	T_y	η_H	P
0.4%	0.4%	0.6%	1.4%

Table 2
Predictions of our model for the main parameters of the hybrid solar gas-turbine plant developed for the SOLUGAS project [7,46]. The elected parameters for the simulation of the combustion chamber and solar subsystems are shown (the working temperature of the solar collector, T_{HS}, was obtained from an energy balance, see text for details and references). All other parameters for the gas-turbine itself are those contained in Table 1.

Combustion related parameters			
$\eta_C = 0.98$	$T_{HC} = 1430$ K	$\varepsilon_{HC} = 0.98$	
Solar plant parameters			
$\eta_0 = 0.73$	$T_{HS} = 1088$ K	$\varepsilon_{HS} = 0.95$	$G = 860$ W/m^2
$\alpha = 0.1$	$\sigma = 5.67 \times 10^{-8}$ W/(m^2 K^4)	$C = 425.2$	$U_L = 5$ W/(m^2 K)
Estimated output parameters			
$f = 0.42$	$\dot{m}_f = 0.151$ kg/s	$P = 4.2$ MW	
Estimated efficiencies			
$\eta_H = 0.393$	$\eta_S = 0.697$	$\eta = 0.317$	$r_e = 0.647$

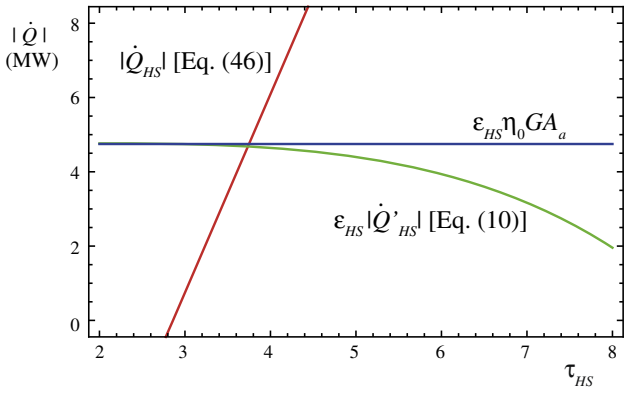

Fig. 5. Energy balance in order to obtain the working temperature of the solar collector, by using Eqs. (10) and (46). The useful energy per unit time that the solar collector could ideally release (no losses), $\epsilon_{HS}\eta_0 GA_a$ is also displayed. So, the difference between the blue and the green curve accounts for the heat transfer losses at the solar collector. (For interpretation of the references to colour in this figure legend, the reader is referred to the web version of this article.)

and were achieved in previous similar plant prototypes. The crossing point corresponds to a thermal energy delivery to the turbine about 5 MW, that also is in accordance with the experimental measures.

With respect to the combustion chamber a standard combustion efficiency, η_C, heat exchanger efficiency, ε_{HC}, and temperature inside the chamber for natural gas, T_{HC} (see Table 2) were taken. Some estimated output parameters as well as predicted efficiencies are shown at the bottom of Table 2. The obtained turbine inlet temperature, T_3, and power output, P, corresponds to the expected for the considered turbine. The corresponding solar share is obtained directly from its definition and the rate of fuel mass was obtained by assuming a lower heating value for natural gas of $Q_{LHV} = 47.141$ MJ/kg [42]. It should be stressed that the global efficiency of the plant, $\eta = 0.317$, is a perfectly reasonable value for the peak efficiency of this kind of plants [43].

4. Sensitivity analysis

In this section the sensitivity of the main output records to some basic design parameters of the heat engine itself as regenerator efficiency, ε_r, turbine and compressor isentropic efficiencies, ε_t and ε_c, and the pressure losses in the heat absorption process, ρ_H is analyzed. In Fig. 6 it is depicted the influence of variations of $\varepsilon_r, \varepsilon_t$ and ε_c on the heat engine efficiency, η_H, the fuel consumption efficiency, r_e, the overall plant efficiency, η, and the power output, P. Design point (DP) conditions are those contained in Tables 1 and 2. In the horizontal axis, percentage variations up to 10% on several losses parameters are represented (denoted in general as $\Delta\varepsilon$), and the vertical axis refers to relative variations of the indicated magnitudes with respect to design point output parameters. In real values, the intervals considered for the losses parameters are: $\varepsilon_r, [0.698, 0.853]$; $\varepsilon_t, [0.797, 0.974]$, and $\varepsilon_c, [0.734, 0.897]$. From the figure, it is clear that for all the considered variables, evolutions are almost linear and the slope of the trends is always higher for ε_t, than ε_c. So, globally the plant is more sensitive to the losses in the turbine. For instance, a 10% improvement on ε_t increases the overall efficiency, about 12% and on r_e about 22%. Similarly, if an investment is done in order to improve ε_c in the same amount, η and r_e would increase 10%. And, of course, a simultaneous increase of ε_t and ε_c would lead to a significant increase of all the output records. A 10% increase in both would result in an increase in η around 22% and in r_e about 35%.

With respect to the sensitivity of the plant to changes on the efficiency of the recuperator, ε_r, it can be seen from Fig. 6 that, as expected, P does not depend on it because power is the difference between the net absorbed heat rate and the net heat released to the ambient, and the regeneration process is an internal heat transfer in the cycle. More stressing is the fact that the fuel conversion rate, r_e, presents a quite flat dependence on ε_r, at least for the considered variation interval. In principle, it should be expected that an increase in ε_r would produce a decrease in fuel consumption and thus increase r_e. And the fuel savings should be more important for lower temperatures of the solar collector, once the turbine inlet temperature is fixed. To investigate this point we show in Table 3 r_e for three values of the working temperature of the solar collector, T_{HS} (the design point temperature corresponds to the intermediate one, $T_{HS} = 1088$ K), and several values of ε_r covering the widest possible interval for ε_r, including the limit cases of no regeneration ($\varepsilon_r = 0$) and limit ideal regeneration ($\varepsilon_r = 1$). From the table can be concluded that, actually r_e is sensitive to ε_r, although not so sensitive as one could a priori expect. For instance, for the lowest value of $T_{HS} = 873$ K, the relative increase of r_e between the limit cases of ε_r amounts 2.8%. For T_{HS} at the design point, 4.3%, and in the limit case $\varepsilon_r = 1$, around 9.2%. In terms of the rates of fuel consumption, $\dot{m}_f$, relative fuel savings are similar. In the table real units are shown by considering natural gas as fuel.

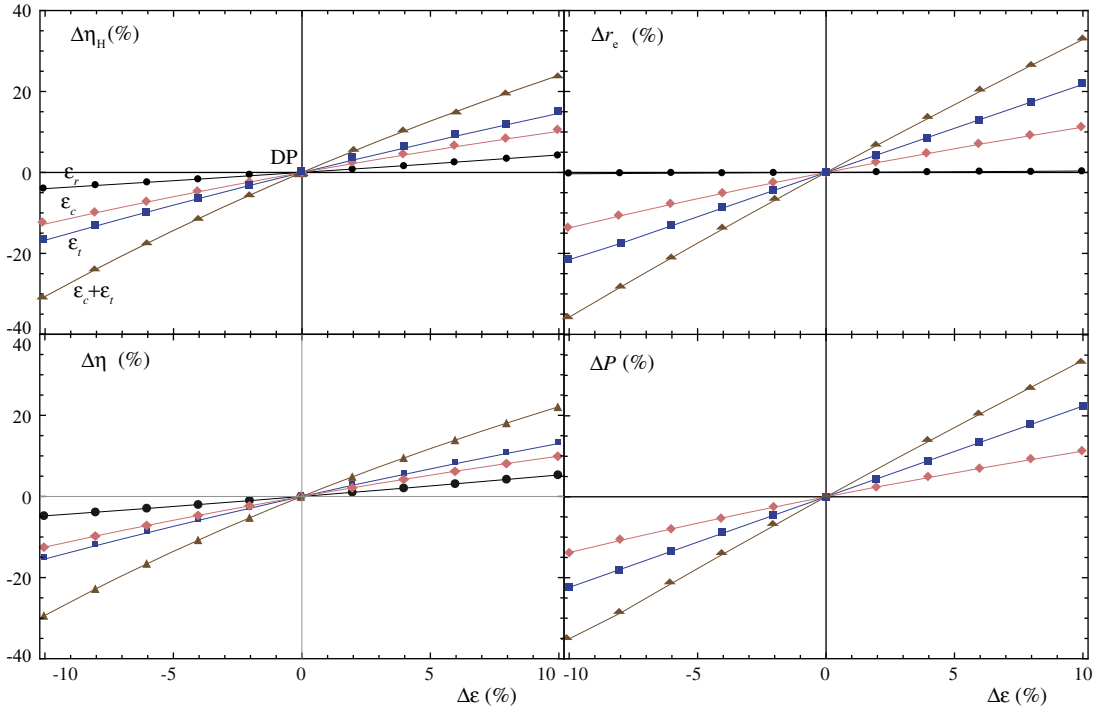

Fig. 6. Sensitivity analysis of the heat engine efficiency, η_H, the fuel conversion rate, r_e, the overall thermodynamic efficiency, η, and the power output, P, to several losses parameters related with the heat engine: regenerator effectiveness, ε_r, compressor and turbine isentropic efficiencies, ε_c and ε_t respectively, and simultaneous variations of both, $\varepsilon_c + \varepsilon_t$. The point $(0, 0)$ corresponds to design point (DP) conditions. In the x axis we represent relative variations of the losses parameters with respect to those at DP, and in the y axis the relative variations of efficiencies with respect to DP.

Table 3
Evolution of the fuel consumption rate, r_e, and the fuel consumption itself, $\dot{m}_f$, with the effectiveness of the regenerator for different working temperatures of the solar collector, T_{HS} (between 600 and 1000 °C). The considered design point corresponds to $\varepsilon_r = 0.775$. The interval $\varepsilon_r = 0.775 - 0.95$ could be taken as realistic for actual regenerators. The cases $\varepsilon_r = 0.0$ and $\varepsilon_r = 1.0$ corresponds to the limit cases of no-regeneration and ideal regeneration respectively.

		$\varepsilon_r = 0.0$	0.775	0.85	0.95	1.0
$T_{HS} = 873$ K	r_e	0.399	0.408	0.409	0.410	0.410
	$\dot{m}_f$ (kg/s)	0.243	0.239	0.238	0.237	0.237
1088 K	r_e	0.624	0.647	0.649	0.652	0.653
	$\dot{m}_f$ (kg/s)	0.157	0.151	0.151	0.150	0.150
1273 K	r_e	1.203	1.288	1.296	1.308	1.314
	$\dot{m}_f$ (kg/s)	0.082	0.076	0.076	0.075	0.075

With respect to the sensitivity of the plant to the pressure losses during the heat absorption process, Fig. 7 shows the relative variations of the power output and efficiencies against the relative variations of the pressure losses, considered as a global parameter, including those losses associated to the heat absorption from the solar collector and those from the combustion chamber. In future works this could be investigated more deeply by considering different losses in both heat absorption processes. From the figure it could be concluded that, as a limit ideal situation, the total elimination of pressure losses will increase power output, P, and fuel conversion rate, r_e, about 10%, and the overall plant efficiency about 7%.

5. Results and conclusions

Next, the influence of the ambient temperature, T_L, on the solar share, f, and on the gas temperature at the recuperator exit, T_y are analyzed. Ambient temperature is a key parameter because it simultaneously has an effect on the solar collector subsystem and on the heat engine. In Fig. 8(a) T_y is depicted for several values of the recuperator efficiency, ε_r. It is a measure of the eventual possibilities of profiting the residual heat for combining the Brayton cycle with a bottoming one. In the absence of recuperator, $T_y = T_4$ and does not depend on T_L. For the set of parameters considered (those at DP), the exit temperature would be around 900 K. For a recuperated cycle, T_y is always a linearly increasing function of T_L. Its numerical value, obviously, is higher as ε_r decreases. In Fig. 8(b) the solar share, f, is depicted in terms of T_L. Dashed lines are built by fixing all the parameters at DP, except ε_r for which several values between 0.0 and 0.95 are considered. The solar share

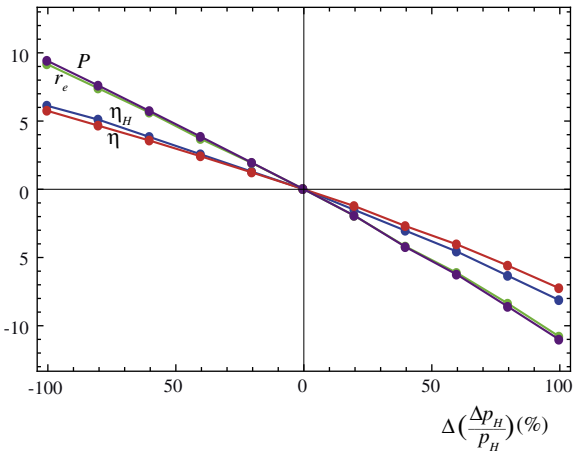

Fig. 7. Relative variations of P, r_e, η, and η_H with respect to DP in terms of relative variations of the pressure losses in the heat absorption process, $\Delta(\Delta p_H/p_H)$.

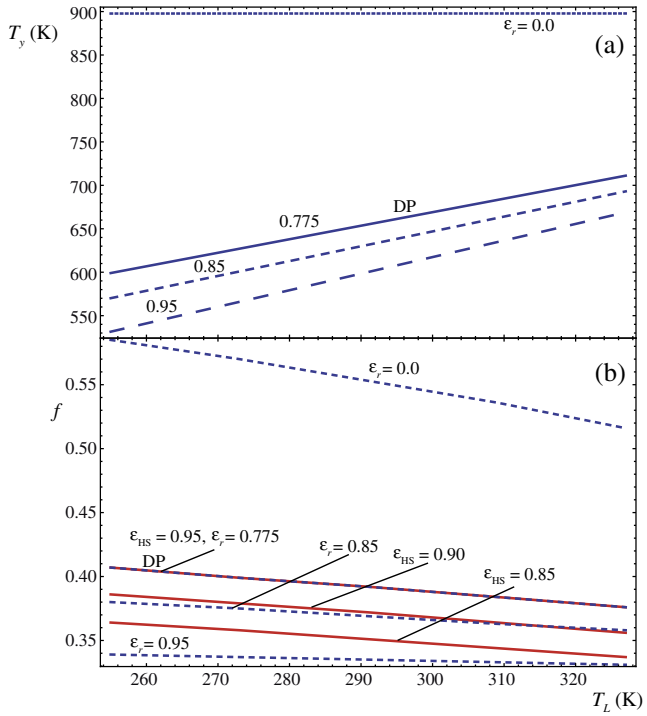

Fig. 8. (a) Evolution with the ambient temperature, T_L, of the temperature of the working fluid at the recuperator exit, T_y, for several values of the recuperator efficiency, ε_r. All the other parameters corresponds to design point. (b) Solar share, f, as a function of the external temperature. Dashed lines show the evolution with ε_r if all other parameters are fixed at DP conditions. Solid lines show the evolution with the effectiveness of the heat exchanger of the solar subsystem, ε_{HS}. The lines marked with DP corresponds to all parameters at design point.

always decreases with T_L, and as the effectiveness of the regenerator increases (and thus the temperature, T_x) its numerical values decrease because the solar heat input required to reach the turbine inlet temperature is lower. Solid curves in Fig. 8(b) are obtained by taking several values of ε_{HS} and considering all the rest at DP. As it should be expected, in this case numerical values of f are higher as ε_{HS} increases because the solar heat input is more efficiently transferred to the gas.

The evolution of the global efficiency, η, and the fuel conversion rate, r_e, with the pressure ratio of the Brayton cycle and the temperature ratios associated to combustion, τ_{HC}, and to the solar collector τ_{HS} are depicted in Figs. 9 and 10. All the plots shown in these figures exhibit a maximum in terms of r_p, so both efficiencies are susceptible to be optimized in terms of r_p. It is not the objective of this paper to perform a detailed optimization analysis. The model presented in this work, although analytical and depending on a relatively reduced number of variables, would require a multi-parametric optimization analysis [25,44,45] in order to obtain realistic conclusions. It is only intended here to check the evolution of η and r_e with three key parameters: the pressure ratio of the turbine and the mentioned temperature ratios.

The overall efficiency (see Fig. 9) numerically increases as τ_{HC} does (from top to bottom in the figure). An approximately realistic interval of values of τ_{HC} was considered (the highest one is slightly above the metallurgic limit for actual turbines), including particularly the design point one for the plant considered in Section 3. Some of the curves are cut at small values of r_p because the solar share, f, becomes negative. For a fixed value of τ_{HC}, an increase in the solar collector temperature ratio, τ_{HS}, causes a decrease in the overall efficiency. This is associated to the monotonic decrease of the solar efficiency, η_s, with τ_{HS}, Eq. (11). On the contrary, the effect of τ_{HS} on the fuel conversion rate, r_e, is opposite: for a fixed

combustion temperature, it increases with increasing τ_{HS}. In other words, from the perspective of decreasing fuel consumption, evidently a higher temperature for the solar collector is preferable. Although from a thermodynamic viewpoint, overall efficiency behaves opposite. In both figures the design point of the SOLUGAS project plant is shown with a red dot. It is interesting the fact that the design point almost coincides with the maximum value of r_e

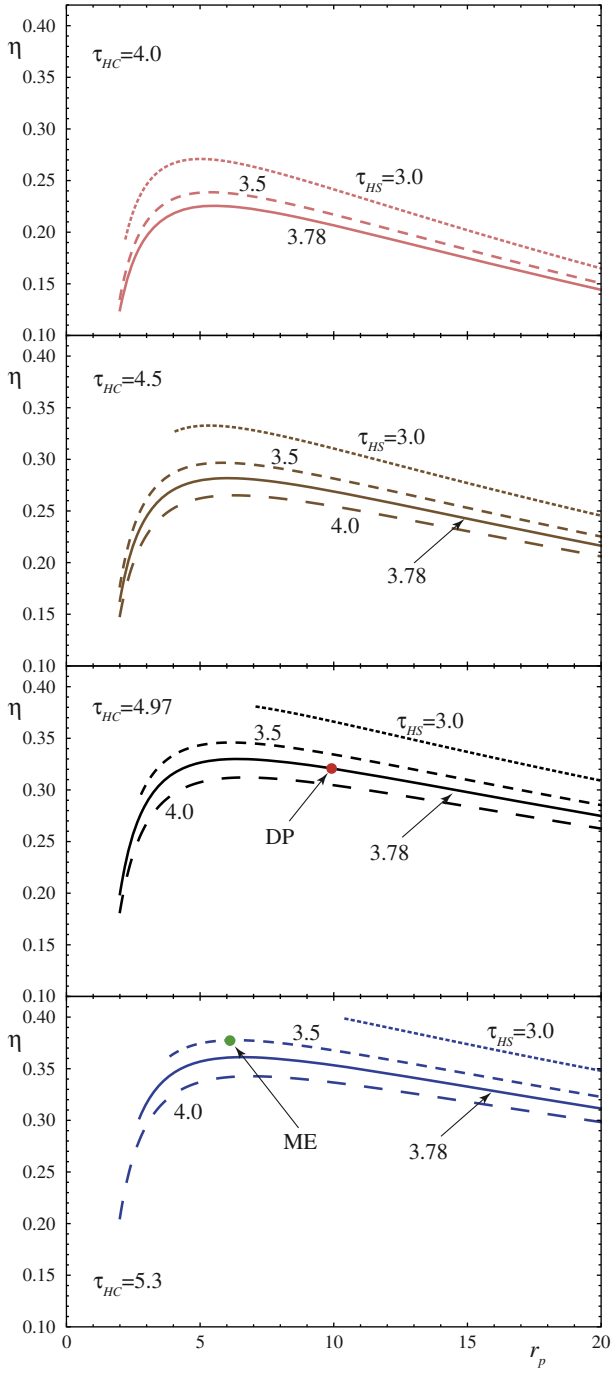

Fig. 9. Evolution of the overall plant efficiency, η, with the pressure ratio, r_p, for several values of the temperature ratio associated to the combustion chamber, τ_{HC} and that associated to the solar collector, τ_{HS}. Design point conditions (marked with a red dot) correspond to $\tau_{HC} = 4.97$, $\tau_{HS} = 3.78$, and $r_p = 9.9$. Curves are shown in the intervals where the solar share, f, reaches positive values. The maximum efficiency (ME) point is displayed at the bottom panel. (For interpretation of the references to colour in this figure legend, the reader is referred to the web version of this article.)

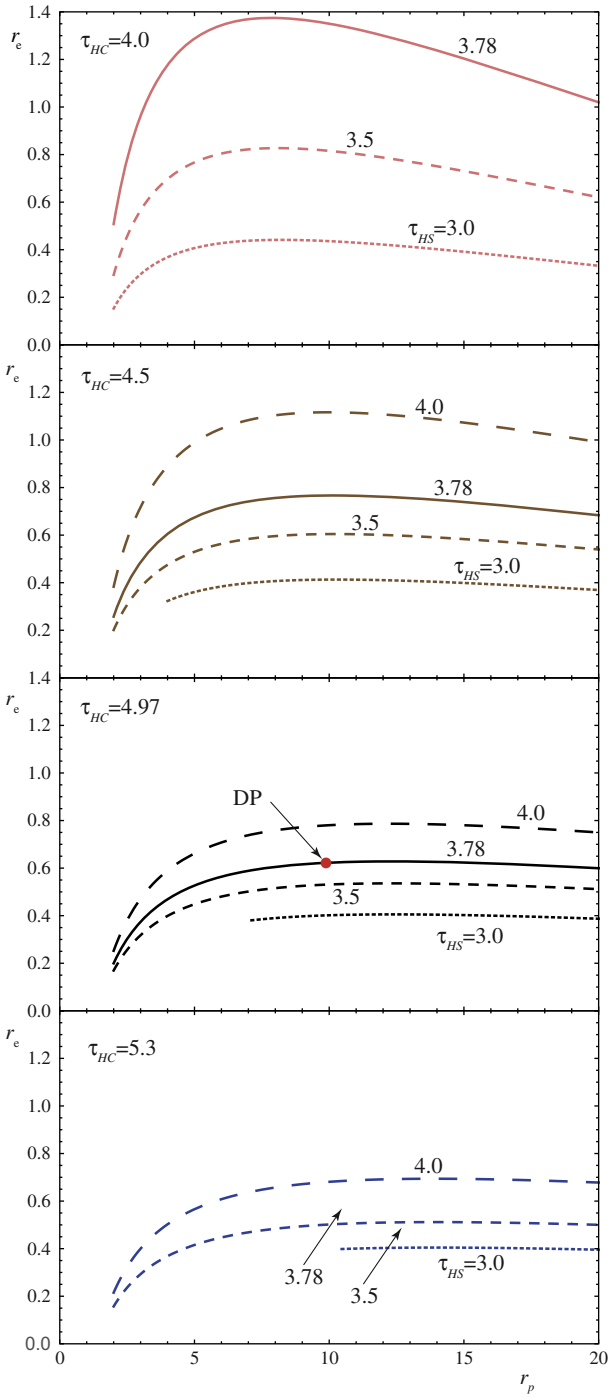

Fig. 10. Same that Fig. 8 for the fuel conversion rate, r_e. Note that the design point for the SOLUGAS project (red dot) is very close to the maximum value of r_e for the corresponding values of τ_{HC} and τ_{HS}. (For interpretation of the references to colour in this figure legend, the reader is referred to the web version of this article.)

for the considered values of the temperature ratios. This means, that one of the main objectives by the designers of the SOLUGAS project in taking the main plant parameters is precisely associated to minimize fuel consumption for the required power output, P.

In the bottom panel of Fig. 9 the maximum efficiency point is shown (the curve corresponding to $\tau_{HS} = 3.0$ is not considered because it does not display a maximum in the r_p interval leading to positive values of the solar share, i.e., the system would not work in a hybrid mode). This maximum efficiency conditions are: $\tau_{HS} = 3.5, \tau_{HC} = 5.3$, and $r_p = 6.1$. The corresponding values of

efficiencies and the main cycle temperatures are shown in Table 4. The overall efficiency at this point is a 19% higher than that at the design point.

Fig. 11 shows the curves of P for the same cases that in Figs. 9 and 10. Power output increases with τ_{HC} (*i.e.* with an increase in the turbine inlet temperature) but is almost insensitive to the working temperature of the solar collector (provided that the combustion chamber ensures to reach the intended turbine inlet temperature). The design point is close to the maximum achievable power for the experimental temperature ratios. It is also shown the maximum power output point. From the data in Table 4 in this point almost a 30% increase of the power output with respect to the design point. Anyway, it should be noted again that a rigorous optimization analysis of the model presented in this work would require multi-parametric optimization techniques. Work along this line is in progress.

The solar share, f, *i.e.*, the fraction of the total heat input absorbed from the solar collector does not present a maximum as a function of r_p for any of the considered combinations of τ_{HC} and τ_{HS} (see Fig. 12). As τ_{HC} increases (from top to bottom in the figure) the solar share decreases. For a fixed value of τ_{HC}, it increases with the temperature of the solar collector. So, f is closer to 1 (pure solar heat input) for high values of τ_{HS} and small combustion temperatures. In numerical terms, it does not reach the value $f = 0.8$ for any of the cases checked. The interval of values of r_p leading to positive f narrows with increasing τ_{HC} and

Table 4
Main temperatures of the Brayton cycle performed by the gas turbine for the design point considered (DP), maximum overall efficiency conditions (ME) and maximum power output (MP). Plant efficiencies, fuel conversion rate (r_e), power output (P) and fuel consumption ($\dot{m}_f$) are also shown.

	ME	DP	MP
T_1 (K)	288	288	288
T_2 (K)	502	579	652
T_x (K)	936	826	826
T'_x (K)	1004	1075	1000
T_3 (K)	1516	1423	1516
T_4 (K)	1063	898	876
T_y (K)	628	650	703
r_p	6.1	9.1	15.0
τ_{HC}	5.3	4.97	5.3
τ_{HS}	3.5	3.78	3.5
η_H	0.413	0.393	0.399
η_S	0.704	0.697	0.704
η	0.378	0.317	0.345
r_e	0.450	0.647	0.511
P (MW)	4.72	4.18	5.42
$\dot{m}_f$ (kg/s)	0.223	0.151	0.225

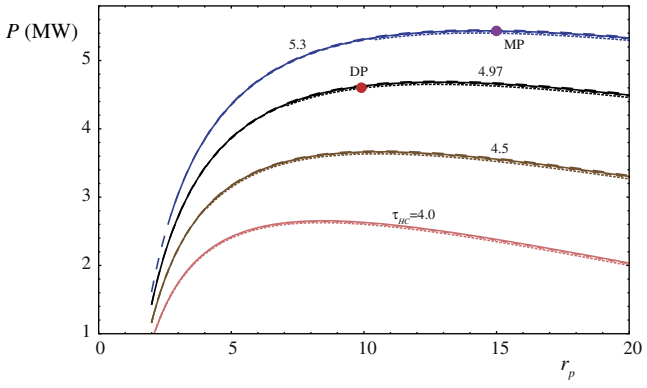

Fig. 11. Same that Figs. 8 and 9 for the power output in real units, P. The figure shows that power output is almost insensitive to changes in τ_{HS}. The maximum power output (MP) and design (DP) points are shown.

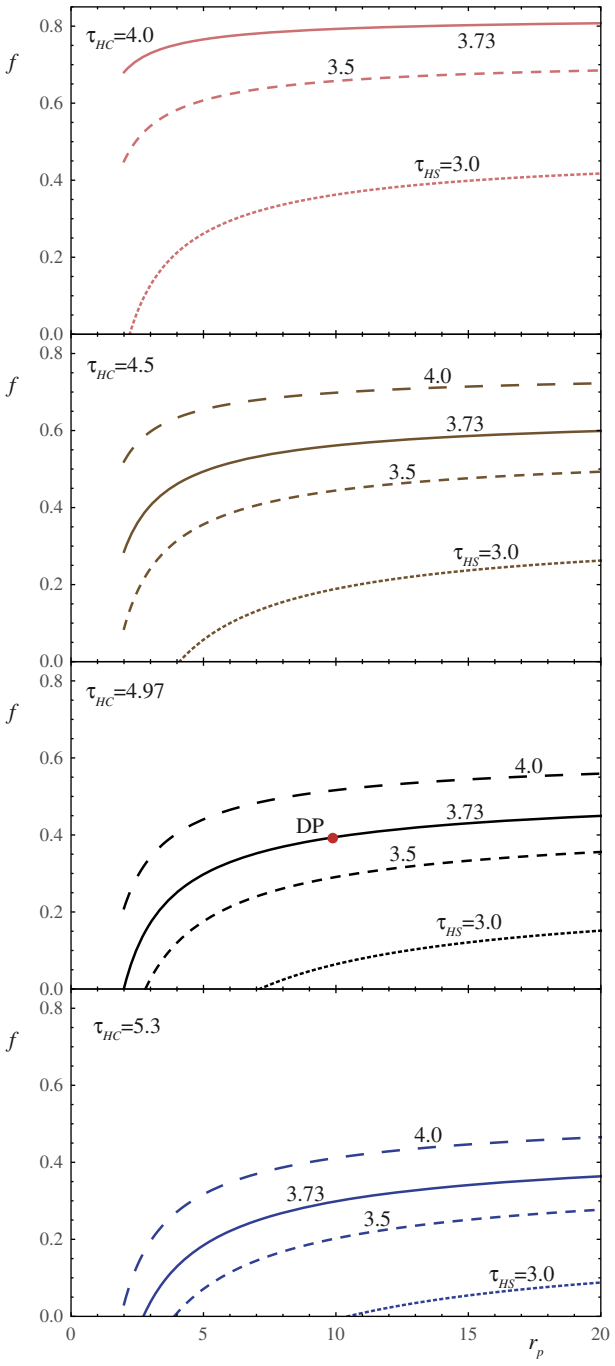

Fig. 12. Evolution of the solar share, f, with the pressure ratio, r_p, for several values of τ_{HC} and τ_{HS}. Design point conditions (marked with a red dot) correspond to $\tau_{HC} = 4.97$, $\tau_{HS} = 3.78$, and $r_p = 9.9$. (For interpretation of the references to colour in this figure legend, the reader is referred to the web version of this article.)

decreasing τ_{HS}. For instance, by looking at the bottom panel of the figure ($\tau_{HC} = 5.3$) it is concluded that for $\tau_{HS} = 3$ the solar share is only positive (*i.e.*, the solar collector really contributes to the heating of the working fluid) for r_p above approximately 10. Globally, for working temperatures of the solar collector not too high, it would preferable to design the plant with a relatively high pressure ratio.

In summary, we have presented in this work a thermodynamic model for a hybrid thermosolar gas-turbine power plant. The model includes the main irreversibility sources from all the subsystems that form the global system. It allows to obtain analytical expressions for the output parameters as power and efficiency, and

eventually other magnitudes. It can be applied to any working mode of the plant, from the hypothetical case in which solar irradiance is enough to reach the turbine inlet temperature, to the case of total absence of solar irradiance and, in consequence, all the heat input coming from a combustion chamber, and the hybrid cases in between.

The system was validated by comparing the predicted values of several variables with those of a commercial turbine. The comparison probed that the model can satisfactorily predict results close to those of real plants. As the model is analytical in nature, in principle, it opens the doors to future works in order to check the influence of several parameters, and so to predict which are the key loss sources in real systems. This can be done from the viewpoint of the solar subsystem, analyzing the influence of variables such as the effective solar collector temperature or heat transfer losses terms. The losses coefficients associated to the components of the gas-turbine itself could also be analyzed. Moreover, analyses in reference to combustion details as the fuel to be burned or peculiarities of the combustion chamber could be also performed in the future. Going a little bit further our model can be used as starting point for optimization analyses, by choosing one or several particular objective functions to be optimized and those design or functioning variables susceptible to be modified in order to obtain the optimum output records. This should be done in the framework of multi-objective multi-parametric optimization techniques as a consequence of the existence of several variables and objective functions to be simultaneously analyzed. This analysis could report useful guidelines in the development of future generations of Brayton hybrid solar plants, with the aim to increase its efficiency and reduce fossil fuel consumption to make them interesting for commercial use.

Acknowledgements

A. Medina and A. Calvo Hernández acknowledge financial support from MINECO of Spain, Grant ENE2013-40644-R, and Universidad de Salamanca.

References

[1] Jamel M, Abd Rahman A, Shamsuddin A. Advances in the integration of solar thermal energy with conventional and non-conventional power plants. Rene Sust Energ Rev 2013;20:71–81.
[2] Schwarzbözl P, Buck R, Sugarmen C, Ring A, Marcos Crespo M, Altwegg P, et al. Solar gas turbine systems: design, cost and perspectives. Sol Energy 2006;80:1231–40.
[3] SOLGATE. Solar hybrid gas turbine electric power system. Tech. rep. EUR 21615, European Commission; 2005.
[4] Sinai J, Sugarmen C, Fisher U. Adaptation and modification of gas turbines for solar energy applications. In: Proceedings of GT2005 ASME Turbo Expo 2005; 2005.
[5] Heller P, Pfänder M, Denk T, Tellez F, Valverde A, Fernandez J, et al. Test and evaluation of a solar powered gas turbine system. Sol Energy 2006;80:1225–30.
[6] Solar-hybrid power and cogeneration plants. Tech. rep., European Commission; 2011. <ordis.europa.eu/publication/rcn/13318_en.html>.
[7] Korzynietz R, Quero M, Uhlig R. SOLUGAS-future solar hybrid technology. Tech. rep., SolarPaces; 2012. <http://cms.solarpaces2012.org/proceedings/paper/7ee7e32ece8f2f8e0984d5ebff9d77b>.
[8] Eck M, Zarza E, Eickhoff M, Rheinländer J, Valenzuela L. Applied research concerning the direct steam generation in parabolic troughs. Sol Energy 2003;74:341–51.
[9] Sogut OS, Durmayaz A. Performance optimization of a solar-driven heat engine with finite-rate heat transfer. Renew Energ 2005;30:1329–44.
[10] Kalagirou S. Solar thermal collectors and applications. Prog En Comb Sci 2004;30:231–95.
[11] Koyun A. Performance analysis of a solar-driven heat engine with external irreversibilities under maximum power and power density condition. Energ Convers Manage 2004;45:1941–7.
[12] Ust Y. Effects of combined heat transfer on the thermo-economic performance of irreversible solar-driven heat engines. Renew Energ 2007;32:2085–95.
[13] Bädescu V. Optimum operation of a solar converter in combination with a Stirling or Ericsson heat engine. Energy 1992;17:601–7.
[14] Frost T, Anderson A, Agnew B. A hybrid gas turbine cycle (Brayton/Ericsson): an alternative to conventional combined gas and steam power plant. Proc Inst Mech Eng Part A 1997;211:121–31.
[15] Blank D, Wu C. Finite-time power limit for solar-radiant Ericsson engines in space applications. Appl Therm Eng 1998;18:1347–57.
[16] Zhang Y, Lin B, Chen J. The unified cycle model of a class of solar-driven heat engines and their optimum performance characteristics. J Appl Phys 2005;97:084905.
[17] Zheng S, Chen J, Lin G. Performance characteristics of an irreversible solar-driven Braysson heat engine at maximum efficiency. Renew Energ 2005;30:601–10.
[18] Wu L, Lin G, Chen J. Parametric optimization of a solar-driven Braysson heat engine with variable heat capacity of the working fluid and radiation-convection heat losses. Renew Energ 2010;35:95–100.
[19] Chen J, Yan Z, Chen L, Andresen B. Efficiency bound of a solar driven stirling heat engine system. Int J Energ Res 1998;22:805–12.
[20] Kaushik SC, Kumar S. Finite time thermodynamic evaluation of irreversible Ericsson and Stirling heat engines. Energ Convers Manage 2001;42:295–312.
[21] le Roux W, Bello-Ochende T, Meyer J. Operating conditions of an open and direct solar thermal Brayton cycle with optimised cavity receiver and recuperator. Energy 2011;36:6027–36.
[22] le Roux W, Bello-Ochende T, Meyer J. Thermodynamic optimisation of the integrated design of a small-scale solar thermal Brayton cycle. Int J Energ Res 2012;36:1088–104.
[23] Le Roux W, Bello-Ochende TMJ. The efficiency of an open-cavity tubular solar receiver for a small-scale solar thermal Brayton cycle. Energ Convers Manage 2014;84:457–70.
[24] Le Roux W, Bello-Ochende TMJ. A review on the thermodynamic optimisation and model of the solar thermal Brayton cycle. Renew. Sust. Energ. Rev. 2013;28:677–90.
[25] Spelling J, Favrat D, Martin A, Augsburger G. Thermoeconomic optimization of a combined-cycle solar tower plant. Energy 2012;41:113–20. http://dx.doi.org/10.1016/j.energy.2011.03.073.
[26] Spelling J. Hybrid solar gas-turbine power plants. Ph.D. thesis, KTH Royal Institute of Technology, Department of Energy Technology, Stockholm, Sweden; 2013.
[27] Barigozzi G, Bonetti G, Franchini G, Perdichizzi A, Ravelli S. Thermal performance prediction of a solar hybrid gas turbine. Sol Energy 2012;86:2116–27.
[28] Zhang Y, Lin B, Chen J. Optimum performance characteristics of an irreversible solar-driven Brayton heat engine at the maximum overall efficiency. Renew Energ 2007;32:856–67.
[29] Sánchez-Orgaz S, Medina A, Calvo Hernández A. Thermodynamic model and optimization of a multi-step irreversible Brayton cycle. Energ Convers Manage 2010;51:2134–43.
[30] Sánchez-Orgaz S, Medina A, Calvo Hernández A. Maximum overall efficiency for a solar-driven gas turbine power plants. Int J Energ Res 2013;37:1580–91. http://dx.doi.org/10.1002/er.2967.
[31] Sánchez-Orgaz S, Medina A, Calvo Hernández A. Recuperative solar-driven multi-step gas turbine power plants. Energy Convers Manage 2013;67:171–8.
[32] Heywood J. Internal combustion engine fundamentals. McGraw-Hill; 1988.
[33] Bejan A. Advanced engineering thermodynamics. New Jersey: Wiley Hoboken; 2006.
[34] Duffie J, Beckman W. Solar engineering of thermal processes. Hoboken, New Jersey: John Wiley and Sons; 2006.
[35] Xie W, Dai Y, Wang R. Numerical and experimental analysis of a point focus solar collector using high concentration imaging PMMA Fresnel lens. Energ Convers Manage 2011;52:2417–26.
[36] Fraidenraich N, Gordon J, Tiba C. Optimization of gas-turbine combined cycles for solar energy and alternative-fuel power generation. Sol Energy 1992;48:301–7.
[37] Caterpillar ST. <https://mysolar.cat.com/cda/files/126873/7/dsm50pg.pdf>.
[38] Wark K, Richards D. Thermodynamics. 6th Edition. McGraw-Hill; 1998.
[39] Efficiency in electricity generation. Tech. rep., EURELECTRIC Preservation of Resources Working Group's; 2003.
[40] Sunden B. High temperature heat exchangers (HTHE). In: Proceedings of the Fifth International Conference on Enhanced, Compact and Ultra-Compact Heat Exchangers: Science, Engineering and Technology, Hoboken, NJ, USA; 2005.
[41] de Mello P, Monteiro D. Thermodynamic study of an EFGT (externally fired gas-turbine) cycle with one detailed model for the ceramic heat exchanger. In: Proceedings of ECOS 2011 conference, Novi Sad, Serbia; 2011.
[42] GREET. The greenhouse gases, regulated emissions and energy use in transportation model. Tech. rep., Argonne National Laboratory, Argonne, IL; 2010. <http://greet.es.anl.gov>.
[43] Behar O, Khellaf A, Mohammedi K. A review of studies on central receiver solar thermal power plants. Rene Sust Energ Rev 2013;23:12–39.
[44] Besarati S, Atashkari K, Jamali A, Hajiloo A, Nariman-zadeh N. Multi-objective thermodynamic optimization of combined Brayton and inverse Brayton cycles using genetic algorithms. Energ Convers Manage 2010;51:212–7.
[45] Al-Sood M, Matrawy K, Abdel-Rahim Y. Optimum parametric performance characterization of an irreversible gas turbine Brayton cycle. Int J Energ Env Eng 2013;4:37.
[46] Romero M, Buck R, Pacheco E. An update on solar central receiver systems, projects, and technologies. Tran ASME 2002;124:98.